


Universal nomogram for the atomtronic quantum rotation sensor

Ehsan Arabahmadi, Daniel Schumayer^{✉,*} and David A. W. Hutchinson[✉]

Dodd-Walls Centre for Photonic and Quantum Technologies, Department of Physics, University of Otago, Dunedin, New Zealand

 (Received 3 November 2020; revised 29 March 2021; accepted 30 March 2021; published 16 April 2021)

Bose-Einstein condensates in annular geometries have received significant attention due to their potential use as interferometers for inertial sensing and other applications. We systematically study the critical velocity of a barrier for vortex formation in such a geometry. More significantly, we are able to show that the details of the critical velocity can be captured by a simple analytic solution which can be considered the atomtronic analog of the usual nomographic equations for electronic circuit components. Experimentally useful nomograms can be plotted from the main result of this paper, from the analytic expression abbreviated as Δ , whose accuracy has been validated via full simulations. It is a function of the potential parameters only and it can be used to directly determine parameter regimes for a given application.

DOI: [10.1103/PhysRevA.103.043319](https://doi.org/10.1103/PhysRevA.103.043319)

I. INTRODUCTION

Ultracold atomic circuits have been realized in toroidal condensates with a tunable weak link [1–4]. Annular superfluids with a weak barrier inside can be used as nonlinear interferometers, and thus allow the construction of high-precision quantum devices (cf. Superconducting QUantum Interference Devices (SQUIDs)) or highly sensitive rotation sensors [5–7].

Initially, experiments with superfluids were conducted with liquid helium [8–11], including some utilizing an annular geometry [12–20]. More recently, ring-shaped Bose-Einstein condensates in toroidal traps have been the subject of many experimental and theoretical investigations [21–29] which study persistent currents [1,30,31], solitary waves [24,32], weak links [2,3,33], and the decay of the persistent current via phase slips [34–36]. A persistent flow and controlled creation of phase slips can be created by transferring angular momentum from an optical field or by stirring the superfluid with a barrier. As the rotation rate, Ω , increases from zero up to a few hertz, so does the winding number. Wright *et al.* [3] provided a 1D model for the analysis of such experimental observations and gave an insight into the origin of the critical current within the barrier. However, a detailed analysis of the excitation of vortices and their dynamics in the critical regime is beyond the scope of that 1D model and requires a 2D or 3D model [37,38].

The earliest experiments used simply connected condensates; the perturbing potential moved through the condensate [39–44], used a phase imprinting technique [45,46], or the entire trap was rotated [47–49] to create topologically new excitations, such as vortices or dark solitons. Condensates in annular setups, however, by design, break topological connectedness and the interplay of geometry and physics can be investigated more directly [50–52].

Ramanathan *et al.* [2] have already reported measurements of a critical velocity in a superfluid ring by observing the decay of a persistent current flowing past a stationary optical barrier of varying strengths. Wright *et al.* [3] identified discrete phase slips in a ring geometry perturbed by a moving barrier, although the barrier angular speed was much lower than the local speed of sound.

We focus on the determination of the critical angular speed, Ω_{crit} , above which vortices are created in annular condensates perturbed by a sweeping barrier (see Fig. 1). We investigate the effects of barrier height and azimuthal width. An effective one-dimensional model is also introduced which captures essential features of the annular two-dimensional system. We further reduce this 1D model to an algebraic equation whose discriminant determines the critical angular speed for vortex nucleation. We consider this algebraic equation as the atomtronic analog of the characteristic curves of a nonlinear electronic component, whose working point lies along this curve.

II. MODEL

In an inertial reference frame, the dimensionless Gross-Pitaevskii equation

$$i \frac{\partial \psi}{\partial t} = \left[-\frac{1}{2} \nabla^2 + V(t) + g|\psi|^2 - \Omega L_z \right] \psi \quad (1)$$

describes a system of N interacting bosons at zero temperature. The ΩL_z term allows us to work in a reference frame rotating with a frequency Ω relative to the inertial laboratory frame. For the 2D simulation [53,54], we used $g = 1000$ and a potential, $V(t)$, which is the sum of a stationary, ring-shaped trap, V_t ,

$$V_t(r) = \frac{V_0}{2} \left[\tanh\left(\frac{R_1 - r}{b}\right) + \tanh\left(\frac{r - R_2}{b}\right) + 2 \right],$$

*Corresponding author: daniel.schumayer@otago.ac.nz

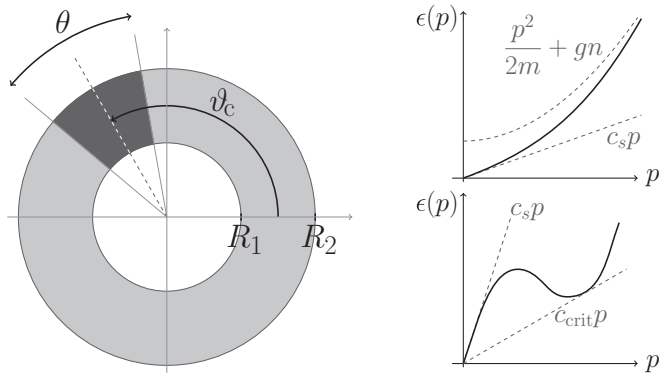


FIG. 1. Left: Overview of the ring-shaped confining trap (gray) with a barrier (dark gray) covering the entire channel width. Top right: The Bogoliubov energy-spectrum of a weakly interacting Bose gas with the speed of sound coinciding with the critical speed as defined by Landau. Bottom right: In the strong interaction regime, the critical speed can be lower than the speed of sound, provided $\epsilon(p)$ develops a local minimum.

and a time-dependent stirring barrier, $V_b(t)$,

$$V_b(\vartheta, t) = \frac{V_b^{\max}}{4} \left[1 + \tanh\left(\frac{1}{b} \left[\vartheta - \vartheta_c(t) + \frac{1}{2}\theta \right] \right) \right] \times \left[1 - \tanh\left(\frac{1}{b} \left[\vartheta - \vartheta_c(t) - \frac{1}{2}\theta \right] \right) \right].$$

Above V_b^{\max} is height/strength of the stirrer barrier and θ is its azimuthal width. The center of the barrier is specified by $\vartheta_c(t)$, which depends on time. The other parameter values are $V_0 = 100$, $R_1 = 2$, $R_2 = 3$, $b = 10^{-2}$, while the barrier height falls in the range of $[0, V_0]$. The strength of the confining ring-potential, V_0 , equates to approximately 21 nK, while the other parameter values correspond to a condensate of sodium atoms with atomic mass of $m = 3.82 \times 10^{-26}$ kg, s -wave scattering length of $a_s = 2.75$ nm. The length- and timescale are determined by $a_0 = 1 \mu\text{m}$, and $\omega_m \approx 2762$ Hz, respectively. The total particle number is kept at $N = 2.9 \times 10^4$.

III. APPEARANCE OF VORTICES

The condensate is prepared in the ground state inside a potential trap with the stationary barrier present. The barrier then starts rotating anticlockwise (positive direction) with a constant angular acceleration of $d\Omega/dt = 0.04$. This small value is chosen to avoid shock-waves and immediate turbulence at the edges, although at sufficiently high speeds the initial ground state becomes unstable against excitations, such as vortices [55].

Superfluid flow in a simply connected domain must be irrotational due to the single-valuedness of the wave function. To increase vorticity within the condensate, a vortex should penetrate into it from outside or an antivortex should do so from the central area of the annulus. Initially, no vortex or antivortex is present, thus such transfer is impossible without the nucleation of vortex pairs in the first place. As an example, Fig. 2 depicts the density and phase in two moments for a barrier ($\theta = \pi/6$), for which vortices enter the depleted region at the trailing edge. The stirring creates an anticlockwise

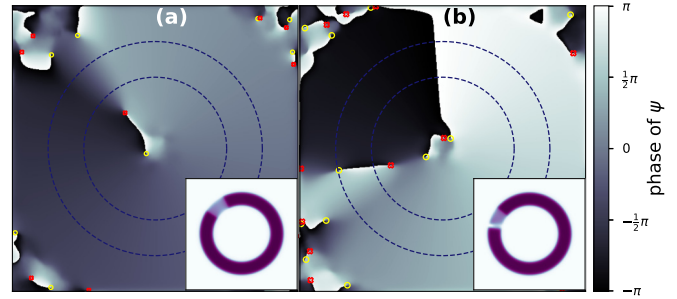


FIG. 2. The phase of ψ is shown at (a) $t = 30000$ and (b) $t = 31040$. Vortices (yellow circles) and antivortices (red crosses) are shown with circles. Insets show the corresponding density profiles. In (b), a vortex is about to enter the bulk of condensate from outside.

current in the channel and a clockwise current through the barrier whose height is smaller than the depth of the trapping potential. The phase increases azimuthally outside the stirrer region and decreases inside of it. The barrier reduces the local density and since the velocity of the superfluid is larger across the barrier, one expects that the condensate reaches its local critical velocity within the barrier region. Indeed, an excitation penetrates into the bulk of the condensate from outside at the trailing edge of the rotating barrier. The critical angular velocity, Ω_{crit} , is estimated by capturing the moment when the vortex/antivortex starts to penetrate the condensate and use the fact that the angular acceleration is constant.

The arguments above explain where vortices may appear relative to the barrier in the azimuthal direction. Here we discuss their appearance in the radial direction and how this depends on the barrier height. At first sight, one may think as follows: The velocity field can be divided into radial and tangential components as

$$\mathbf{v} = \frac{\hbar}{m} \nabla \phi = \frac{\partial \phi}{\partial r} \mathbf{e}_r + \frac{1}{r} \frac{\partial \phi}{\partial \vartheta} \mathbf{e}_\vartheta = \mathbf{v}_r + \mathbf{v}_\vartheta.$$

Assuming that the phase, ϕ , is more or less uniform in the radial direction, as Fig. 2 suggests, the radial velocity $\|\mathbf{v}_r\|$ is more or less constant, while $\|\mathbf{v}_\vartheta\|$ is proportional to r^{-1} . One may expect that a vortex enters from the inner edge, since that has the smaller radius and, consequently, higher $\|\mathbf{v}_\vartheta\|$ which may approach or even becomes higher than the local speed of sound. However, a detailed numerical simulation indicates that there is a threshold height below which a vortex enters from outside, while for barriers stronger than the threshold an antivortex leaves the center and traverses through the condensate.

To understand this effect, the tangential speed $v_\vartheta(r, \vartheta)$ is plotted in Fig. 3 as a function of ϑ at three different radii corresponding to R_1 , to $R_3 \equiv \frac{1}{2}(R_1 + R_2)$, and to R_2 . It is apparent that $v_\vartheta(r, \vartheta)$ within the barrier region has a positive slope, i.e., the velocity at the trailing edge of the barrier is higher than at the leading edge due to the acceleration of the barrier in the azimuthal direction. In fact, this slope vanishes in the absence of barrier acceleration. This seems reasonable, as the leading edge of the barrier compresses the gas a bit, therefore it does not pick up the barrier's speed immediately, while at its trailing edge the barrier leaves a relatively rare volume into which the gas can expand without experiencing resistance,

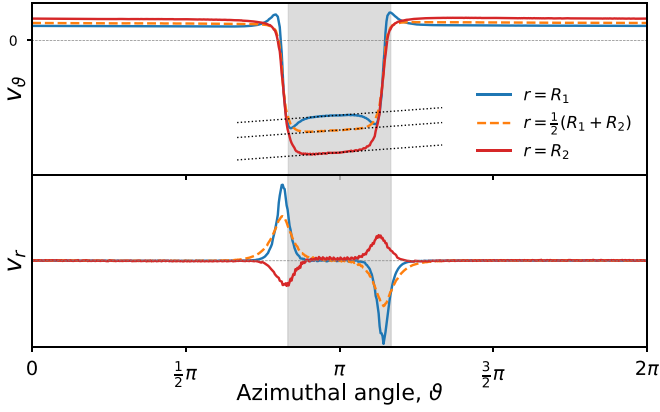


FIG. 3. Azimuthal and radial components of velocity, v_θ and v_r , at $t = 25$ for barrier with height and width of 20 and $\pi/3$, respectively. The angular acceleration is 0.04, thus $v_\theta \approx 1$. The three curves correspond to concentric circles with radii of R_1 (blue solid line developing two small peaks in v_θ on both sides of the shaded area in top figure), of $R_3 = \frac{1}{2}(R_1 + R_2)$ (dashed green line in the middle for v_θ), and of R_2 (red solid line).

thus having higher velocity. This velocity difference explains why the vortex appears behind the barrier.

The interpretation above can be validated by calculating the canonical stress tensor. As the initial condensate does not have spin or intrinsic angular momentum [56], it is sufficient to consider the canonical stress tensor:

$$T^{\alpha\beta} = \sum_r (\partial^\beta \psi_r) \frac{\partial \mathcal{L}}{\partial (\partial_\alpha \psi_r)} - g^{\alpha\beta} \mathcal{L}.$$

Here $\psi_r = (\psi, \psi^*)$, the coordinates are $x^\beta = (t, r, \vartheta)$ with $g_{\alpha\beta} = \text{diag}(+1, -1, -r^2)$, and Lagrangian density:

$$\mathcal{L} = \frac{i}{2} \left[\psi^* \frac{\partial \psi}{\partial t} - \psi \frac{\partial \psi^*}{\partial t} \right] - \frac{1}{2} (\nabla \psi)(\nabla \psi^*) - \frac{g}{2} |\psi|^4 - V |\psi|^2.$$

Figure 4 depicts all nine components of $T^{\alpha\beta}$. The energy density, T^{00} , especially its opposite peaks around the barrier edges, indicates that the gas at the frontal and back sides of the barrier behave differently, partially because of the increased density at the leading edge. It is also noticeable that the energy density (and also the mass density) at $r = R_1$ is somewhat bigger than at $r = R_3$. This difference also points toward vortices entering the bulk of the condensate from the outer perimeter. Similarly, the shear-stress components, $T^{12} = T^{21}$, also show that the highest shear appears at $r = R_3$, both in front and behind the barrier, while in the bulk condensate the shear is much reduced compared to that at R_1 and R_3 . The pressure components, T^{11} and T^{22} , seem to be symmetric on the two sides of the barrier, however, the scale hides minor quantitative differences. At the leading edge, both T^{11} and T^{22} are slightly higher than at the trailing edge, for all three radii.

The fact that the critical velocity of the quantum fluid depends on the local density inside the barrier provides a good method to create controlled numbers of vortices. A vortex depletes a definite region of the condensate and consequently pushes the density elsewhere, increasing the critical velocity for vortex formation. Hence, if the superfluid velocity is just above the previous critical value, it may not be sufficient for

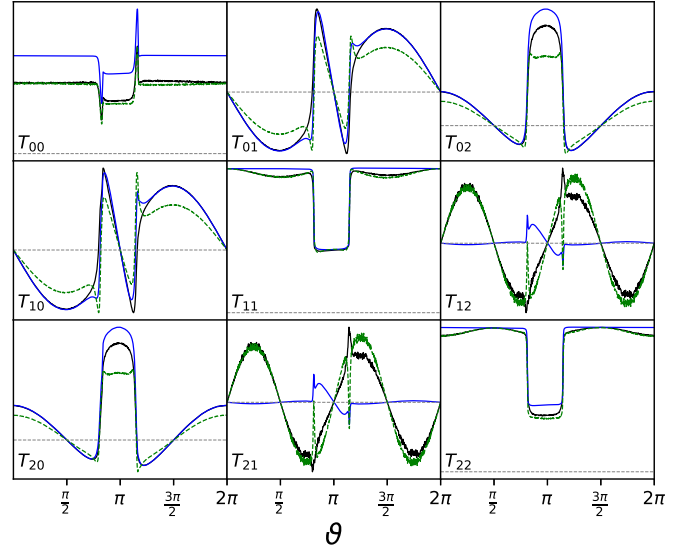


FIG. 4. All elements of the canonical stress tensor, $T^{\alpha\beta}$, are plotted as a function of azimuthal angle for fixed radii, R_1 (black solid middle line in T_{00}), R_2 (blue solid line in T_{00}), and R_3 (dashed green bottom line in T_{00}). The scale of vertical axes in different subplots are different, thus graphs are only comparable within a subplot. The gray dashed line indicates the relevant zero level in each graph.

the increased threshold and the creation of a second vortex is suppressed.

IV. MODEL REDUCTION

In simulating the time evolution of a two-dimensional condensate, we only allowed for small and slow changes, hence the density far from boundaries reaches a constant value. This uniformity allows the reduction of dimensionality and hence we create an *effective* one-dimensional problem, along a circle of radius \bar{r} . Furthermore, the barrier acceleration is negligible, thus we consider the time evolution of the system to be sufficiently slow throughout the entire simulation so we can assume it to be in a stationary state in the corotating frame.

A. Effective one-dimensional model

Let us factorize the wave function as $\psi(r, \vartheta, t) = \Theta(\vartheta, t)P(r)$, where the purely real radial function is defined as

$$P(r) = \left[\int_0^{2\pi} |\psi_{\text{gs}}(r, \vartheta)|^2 r d\vartheta \right]^{1/2},$$

where $\psi_{\text{gs}}(r, \vartheta)$ is the two-dimensional ground state wave function normalized to unity. Its time evolution is then governed by

$$i \frac{\partial \Theta}{\partial t} = \left[-\frac{1}{2\bar{r}^2} \frac{\partial^2}{\partial \vartheta^2} + V + \bar{g} |\Theta|^2 \right] \Theta,$$

in which \bar{r} and \bar{g} are the weighted average of radius and interaction strength

$$\bar{r} = \int_0^\infty r |P(r)|^2 dr \quad \text{and} \quad \bar{g} = g \int_0^\infty |P(r)|^4 dr.$$

where, in both integrals, the limits of 0 and ∞ can be effectively replaced by R_1 and R_2 , respectively. Here we note that calculating the \bar{r}^{-2} factor in the kinetic energy term may seem unwarranted, as one should rather calculate r^{-2} . The difference between these approaches is negligible in our geometry and can also be shown to be at most 5% in the worst case scenario [57].

Unlike the two-dimensional case, here phase slips occur when a dark soliton is created above a critical velocity of the barrier. The critical speed appears to be very close to that found in the two-dimensional analysis, e.g., the parameter set which determines $\Omega_{\text{crit}} = 1.23$ in 2D, leads to $\Omega_{\text{crit}} = 1.21$ in the effective model. This similarity suggests that we may be able to find a simpler model predicting Ω_{crit} than solving the 2D Gross-Pitaevskii equation. First, examine the dynamics in the corotating frame where the governing Eq. (1) becomes

$$\left[-\frac{1}{2\bar{r}^2} \frac{\partial^2}{\partial \vartheta^2} + V + \bar{g}|\Theta(\vartheta)|^2 + i\Omega \frac{\partial}{\partial \vartheta} \right] \Theta(\vartheta) = \varepsilon \Theta. \quad (2)$$

B. Effective algebraic model

Using Euler's relation, we write $\Theta = \sqrt{\rho} e^{i\phi}$. Substituting this into Eq. (2), we obtain a pair of differential equations,

$$\begin{aligned} \phi(\vartheta) &= \bar{r}^2 \Omega \vartheta + \int \frac{J}{\rho(\vartheta)} \bar{r} d\vartheta, \\ 0 &= 2\rho\rho'' - (\rho')^2 - 4J^2 - 8\bar{g}\rho^3 - 8(V(\vartheta) - \mu)\rho^2, \end{aligned}$$

where $\mu = \varepsilon + \frac{1}{2}\bar{r}^2\Omega^2$ and the quantum current in the rotating frame is $J = \rho v = \rho(\nabla\phi + \bar{r} \times \Omega)$. Due to its uniformity, we approximate the density with constant value inside, ρ_b , and outside, ρ_o , of the barrier. This assumption leads to a set of algebraic equations,

$$\begin{aligned} 2\pi\bar{r}\Omega + J \left[\frac{\theta_b}{\rho_b} + \frac{\theta_o}{\rho_o} \right] &= 0, \\ J^2 + 2\rho_b^2(\bar{g}\rho_b + V_b - \mu) &= 0, \\ J^2 + 2\rho_o^2(\bar{g}\rho_o - \mu) &= 0, \\ \bar{r}(\rho_b\theta_b + \rho_o\theta_o) &= 1, \end{aligned}$$

where $\theta_o = 2\pi - \theta_b$, the azimuthal width of the channel outside of the barrier. The last equation guarantees closure and expresses the normalization of the wave function. Eliminating all variables other than the density within the barrier, we obtain

$$A\rho_b^3 + B\rho_b^2 + C\rho_b + D = 0, \quad (3)$$

where the coefficients are

$$\begin{aligned} A &= \frac{64\pi^3 \bar{g} r^2}{\theta_o^3} (\pi - \theta_b)^2, \\ B &= \frac{8\pi^2 \bar{r} (\theta_b - \theta_o)}{\theta_o^3} \\ &\quad \times [(\bar{r}V_b\theta_o - 2\bar{g})(\theta_b - \theta_o) - 2\pi\bar{g} + \pi\bar{r}^3\Omega^2\theta_o], \\ C &= \frac{4\pi\theta_b}{\theta_o^3} [4\bar{r}V_b\theta_o(\theta_o - \pi) + 2\pi\bar{r}^3\Omega^2\theta_o + 5\bar{g}\theta_b - 4\pi\bar{g}], \\ D &= \frac{2}{\bar{r}\theta_o^3} [2\pi^2\bar{r}^3\Omega^2 + V_b\theta_b^2\theta_o - \bar{g}\theta_b^2]. \end{aligned}$$

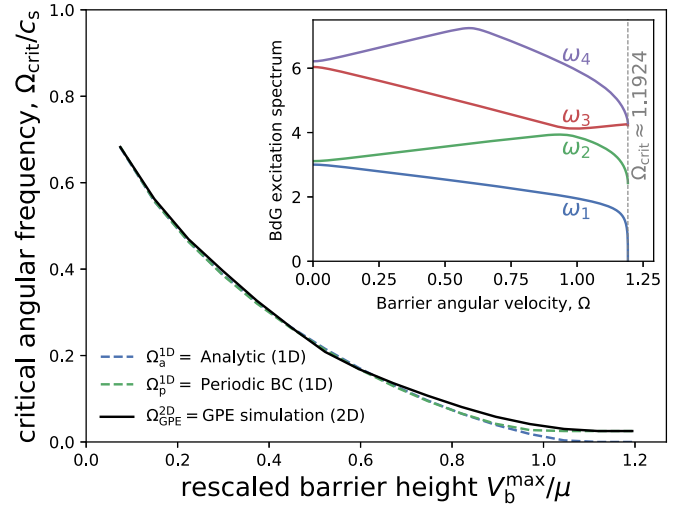


FIG. 5. Critical angular velocity is depicted as a function of barrier height using three different methods: $\Omega_{\text{GPE}}^{2\text{D}}$ is obtained from solving the two-dimensional Gross-Pitaevskii equation (black solid line), while $\Omega_p^{1\text{D}}$ and $\Omega_a^{1\text{D}}$ are derived from the one-dimensional effective Gross-Pitaevskii equation with periodic boundary conditions (dashed green line flattening at a finite value around $V_b^{\text{max}}/\mu \approx 1$) and from the analytic approximation (blue dashed line), respectively. Although μ varies slowly from 61 ($V_b \approx 0$) to 65 ($V_b \approx 70$), one may consider it to be constant around 65 while interpreting the figure. Inset shows the first few lowest excitation frequencies, ω_k , of the Bogoliubov-de Gennes spectrum for a barrier height of 20.

The subscripts, b and o, indicate whether the given quantity is measured inside or outside of the barrier.

C. Predicting Ω_{crit}

Once ρ_b is determined, one can calculate the other unknown quantities, μ , ρ_o , and J , straightforwardly. According to the fundamental theorem of linear algebra, the third-order polynomial (3) has three roots over the complex numbers. Moreover, since the coefficients of the polynomial are all real, the complex roots appear in conjugate pairs. If the determinant

$$\Delta = 18ABCD + B^2C^2 - 4AC^3 - 4B^3D - 27A^2D^2 \quad (4)$$

is positive, there are three purely real solutions, while for $\Delta < 0$ we have one real solution and a complex conjugate pair. Indeed, this sign change of Δ determines Ω_{crit} and thereby signals the regime of the unknown quantities, μ , ρ_o , ρ_b , and J fall in their physically allowed ranges, e.g., all densities are positive.

The polynomial Δ is of degree eight in Ω without a constant term and with only even powers present. Consequently, the equation $\Delta = 0$ has two trivial solutions $\Omega_{1,2} = 0$ and three pairs where the members of each pair have opposite signs. This symmetry simply means that the stirring can either be clockwise or anticlockwise, thus carrying no physically relevant extraneous information. The lowest positive root yields Ω_{crit} , which is in very good agreement with that obtained from the Gross-Pitaevskii equation in two dimensions, and with the one given by the effective 1D equation, Eq. (2). Figure 5 depicts Ω_{crit} determined from all three approaches and the axes are rescaled by the local speed of sound, $c_s = (\beta\rho_b)^{1/2}$, and

by the chemical potential μ . Although the chemical potential changes slowly as V_b increases, in this figure one may consider μ to be approximately 65. The algebraic and the two GPE approaches become qualitatively different for barrier height around unity (in rescaled units), where $(V_b - \mu)$ changes signs, indicating the increasing importance of quantum tunneling. Hence, in practice, the algebraic Eqs. (3) and (4) can be used to determine either the density, if the system is not unstable, or the critical experimental parameters, such as Ω_{crit} , leading to an unstable annular, two-dimensional condensate.

D. Comparison with earlier predictions

Watanabe *et al.* [58] investigated, using the hydrodynamic description within the local density approximation, the corresponding problem for an infinite, homogeneous three-dimensional superfluid flowing in the presence of a potential barrier. There superfluid is under the influence of a one-dimensional confining potential whose maximal value determines the critical current and thus the critical velocity. Facilitating the direct comparison, we have plotted our results measuring Ω_{crit} in the local speed of sound corresponding to the density at the radius R_3 , and using the chemical potential, μ , as a unit for the barrier height. Here we note that μ remains approximately constant for barrier heights below ≈ 66 . While Watanabe *et al.*'s result is comparable to ours, there are important differences as well—mainly, that the system considered here is trapped in an experimentally realizable annular trap, which naturally introduces curvature to the geometry. We also provide the analytic expression explicitly in terms of the potential parameters. By solving the discriminant equation and choosing the physical solution, we obtain

$$\Omega_{\text{crit}}^2 = \frac{1}{4\pi\bar{r}^2} \left[\frac{9\beta^2(\sqrt{3}i - 1)}{\bar{r}\Upsilon} - \frac{(\sqrt{3}i + 1)\Upsilon}{\bar{r}} + 8V_b\hat{\theta}_b - \frac{4\beta}{\bar{r}} \right],$$

where

$$\Upsilon^3 = 27\beta^2 \left(2\bar{r}\sqrt{V_b^2\hat{\theta}_b^2 - \frac{V_b\beta\hat{\theta}_b}{\bar{r}}} + 2V_b\bar{r}\hat{\theta}_b - \beta \right),$$

with the shorthand notation $\hat{\theta}_b = \pi - \theta_b$ for the supplementary angle of θ_b . Figure 6 illustrates the regimes that this model is valid. In terms of the barrier height, it is valid for heights lower than the chemical potential, and in terms of the barrier width, it is valid for barrier widths almost eight times larger than the healing length and also for the region that the function is almost linear. We also compare our numerical results with the predictions for the two limiting cases: thin barriers [59] and wide barriers [60]. In both cases, one may see that the fit is restricted to a narrow region of θ , and for wide barriers the asymptotic prediction in Ref. [60] deteriorates for stronger barriers, i.e., when V_b^{max} becomes comparable with the chemical potential. This is expected as the prediction by Leszczyszyn *et al.* [60] is derived assuming the barriers to be penetrable, while as $V_b^{\text{max}} \approx \mu$ the condensate density decreases exponentially within the barrier. A similar trend is true for the linear fit of our algebraic model; the solid blue lines deviate for wider barriers (see $V_b^{\text{max}} = 40$ and 50 in Fig. 6), although even these give a reasonable fit up to $\theta \approx \frac{\pi}{2}$.

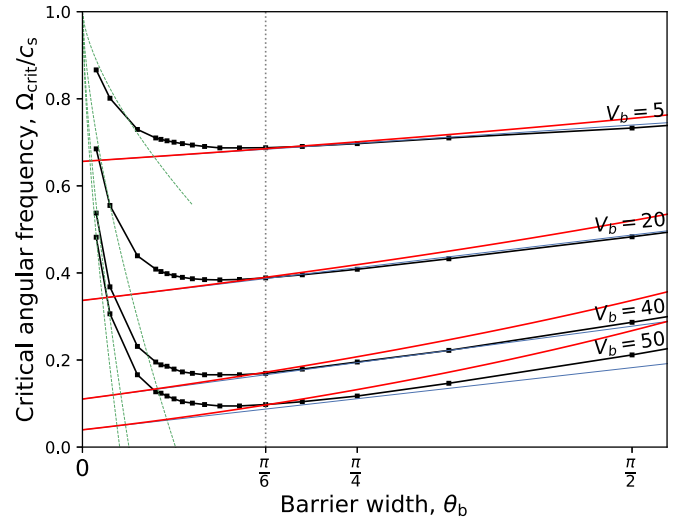


FIG. 6. Critical angular velocity is depicted as a function of barrier width, θ_b , for barrier heights, $V_b^{\text{max}} = 5, 20, 40,$ and 50 . In comparison, the chemical potential $\mu \approx 66.5$ in dimensionless units. The black curves together with the black square markers are the predictions of the 1D Gross-Pitaevskii equation. The red curves correspond to the analytic Ω_{crit} , while the blue straight lines are the linear asymptotes calculated from the algebraic expression as $\theta_b \rightarrow 0^+$. The red curves are always higher than the blue curves. The green dashed lines are the predictions given in Ref. [59] for thin barriers in one dimension.

To verify the prediction of Eq. (4) for Ω_{crit} , we solved for the Bogoliubov–de Gennes excitation spectrum ω_k ($k = 1, 2, \dots$) [61–65] by linearizing Eq. (2) around the stationary solution, Θ_o , assuming that the perturbed wave function has the form $\Theta = \Theta_o + \lambda\Theta_1$. Here $\lambda \ll 1$ and measures the magnitude of perturbation, while $\Theta_1 = u_k(x)e^{-i\omega_k t} + v_k^*(x)e^{i\omega_k^* t}$. Since the Bogoliubov–de Gennes operator is not Hermitian, its spectrum is not guaranteed to be real. The lowest excitation frequency, ω_1 , drops to zero rapidly as $\Omega \nearrow \Omega_{\text{crit}}$, (see inset of Fig. 5), indicating that Θ_o becomes unstable, and a new type of ground state is about to form. This new ground state contains a topological defect: a dark soliton in one-dimension and a vortex in two dimensions.

Overview of atomtronics as an emerging field of quantum technology and, in particular, of the annular setup can be found in review by Amico *et al.* [52].

V. CONCLUSION

We have investigated the mechanisms for a vortex generation in an annular Bose-Einstein condensate slowly stirred by a potential barrier at zero temperature. If the barrier rotates faster than a critical angular velocity, Ω_{crit} , vortices start forming and penetrating into the bulk of the condensate. We have determined Ω_{crit} from the 2D Gross-Pitaevskii equation, from an *effective* 1D Gross-Pitaevskii equation, and from an *algebraic* equation. These approaches agree notably well, up to barrier heights comparable to the main annular trap. The algebraic expression provides an easy path to generate nomograms for this atomtronic circuitry similarly to those used in electronics, where one provides nomograms for nonlinear

components in their corresponding specification sheets, such as for diodes or thermistors.

The determinant, Δ , depends solely on the geometry and physical parameters, hence it is easily adapted to different experimental setups. Here we have demonstrated how to exploit this algebraic equation and the sudden drop of the excitation frequencies, ω_k , in a narrow region around Ω_{crit} . To create a sensitive rotational sensor, the barrier height may be adjusted to tune Ω_{crit} to the rotation speed which one wants to detect. The barrier height seems to be an excellent candidate for such tuning, as its height can finely be modulated by the intensity

of a laser field. However, the algebraic equation allows one to systematically explore the effect of other system parameters on the critical angular velocity and generate a multitude of nomograms similar to Fig. 5.

ACKNOWLEDGMENTS

We acknowledge the financial support from The Dodd-Walls Centre for Photonic and Quantum Technologies. We are grateful to Mark Edwards and Ben Eller (Georgia Southern University) for useful discussions.

-
- [1] C. Ryu, M. F. Andersen, P. Cladé, V. Natarajan, K. Helmerson, and W. D. Phillips, *Phys. Rev. Lett.* **99**, 260401 (2007).
- [2] A. Ramanathan, K. C. Wright, S. R. Muniz, M. Zelan, W. T. Hill, C. J. Lobb, K. Helmerson, W. D. Phillips, and G. K. Campbell, *Phys. Rev. Lett.* **106**, 130401 (2011).
- [3] K. C. Wright, R. B. Blakestad, C. J. Lobb, W. D. Phillips, and G. K. Campbell, *Phys. Rev. Lett.* **110**, 025302 (2013).
- [4] F. Jendrzejewski, S. Eckel, N. Murray, C. Lanier, M. Edwards, C. J. Lobb, and G. K. Campbell, *Phys. Rev. Lett.* **113**, 045305 (2014).
- [5] T. L. Gustavson, P. Bouyer, and M. A. Kasevich, *Phys. Rev. Lett.* **78**, 2046 (1997).
- [6] M. Edwards, *Nat. Phys.* **9**, 68 (2013).
- [7] C. Ryu, P. W. Blackburn, A. A. Blinova, and M. G. Boshier, *Phys. Rev. Lett.* **111**, 205301 (2013).
- [8] F. London, *Nature* **141**, 643 (1938).
- [9] J. F. Allen and A. D. Misener, *Nature* **141**, 75 (1938).
- [10] W. F. Vinen and D. Shoenberg, *Proc. R. Soc. London, Ser. A: Math. Phys. Sci.* **260**, 218 (1961).
- [11] W. J. Trela and W. M. Fairbank, *Phys. Rev. Lett.* **19**, 822 (1967).
- [12] J. D. Reppy, *Phys. Rev. Lett.* **14**, 733 (1965).
- [13] J. R. Clow and J. D. Reppy, *Phys. Rev. Lett.* **19**, 291 (1967).
- [14] P. J. Bendt, *Phys. Rev.* **127**, 1441 (1962).
- [15] P. J. Bendt and R. J. Donnelly, *Phys. Rev. Lett.* **19**, 214 (1967).
- [16] O. Avenel, P. Hakonen, and E. Varoquaux, *Phys. Rev. Lett.* **78**, 3602 (1997).
- [17] K. Schwab, N. Bruckner, and R. Packard, *J. Low Temp. Phys.* **110**, 1043 (1998).
- [18] R. W. Simmonds, A. Marchenkov, E. Hoskinson, J. C. Davis, and R. E. Packard, *Nature* **412**, 55 (2001).
- [19] N. Bruckner and R. Packard, *J. Appl. Phys.* **93**, 1798 (2003).
- [20] E. Hoskinson, Y. Sato, and R. Packard, *Phys. Rev. B* **74**, 100509(R) (2006).
- [21] K. Kasamatsu, M. Tsubota, and M. Ueda, *Phys. Rev. A* **66**, 053606 (2002).
- [22] A. J. Leggett, *Quantum Liquids* (Oxford University Press, Oxford, 2006).
- [23] M. Benakli, S. Raghavan, A. Smerzi, S. Fantoni, and S. R. Shenoy, *Europhys. Lett.* **46**, 275 (1999).
- [24] J. Brand and W. P. Reinhardt, *J. Phys. B: At., Mol. Opt. Phys.* **34**, L113 (2001).
- [25] A. Das, J. Sabbatini, and W. H. Zurek, *Sci. Rep.* **2**, 352 (2012).
- [26] J.-P. Martikainen, K.-A. Suominen, L. Santos, T. Schulte, and A. Sanpera, *Phys. Rev. A* **64**, 063602 (2001).
- [27] J. D. Pritchard, A. N. Dinkelaker, A. S. Arnold, P. F. Griffin, and E. Riis, *New J. Phys.* **14**, 103047 (2012).
- [28] M. Modugno, C. Tozzo, and F. Dalfovo, *Phys. Rev. A* **74**, 061601(R) (2006).
- [29] P. F. Griffin, E. Riis, and A. S. Arnold, *Phys. Rev. A* **77**, 051402(R) (2008).
- [30] S. Beattie, S. Moulder, R. J. Fletcher, and Z. Hadzibabic, *Phys. Rev. Lett.* **110**, 025301 (2013).
- [31] A. I. Yakimenko, K. O. Isaieva, S. I. Vilchinskii, and M. Weyrauch, *Phys. Rev. A* **88**, 051602(R) (2013).
- [32] P. Mason and N. G. Berloff, *Phys. Rev. A* **79**, 043620 (2009).
- [33] K. C. Wright, R. B. Blakestad, C. J. Lobb, W. D. Phillips, and G. K. Campbell, *Phys. Rev. A* **88**, 063633 (2013).
- [34] S. Moulder, S. Beattie, R. P. Smith, N. Tammuz, and Z. Hadzibabic, *Phys. Rev. A* **86**, 013629 (2012).
- [35] F. Piazza, L. A. Collins, and A. Smerzi, *Phys. Rev. A* **80**, 021601(R) (2009).
- [36] F. Piazza, L. A. Collins, and A. Smerzi, *J. Phys. B: At., Mol. Opt. Phys.* **46**, 095302 (2013).
- [37] A. I. Yakimenko, K. O. Isaieva, S. I. Vilchinskii, and E. A. Ostrovskaya, *Phys. Rev. A* **91**, 023607 (2015).
- [38] A. I. Yakimenko, Y. M. Bidasyuk, M. Weyrauch, Y. I. Kuriatnikov, and S. I. Vilchinskii, *Phys. Rev. A* **91**, 033607 (2015).
- [39] C. Raman, M. Köhl, R. Onofrio, D. S. Durfee, C. E. Kuklewicz, Z. Hadzibabic, and W. Ketterle, *Phys. Rev. Lett.* **83**, 2502 (1999).
- [40] R. Onofrio, C. Raman, J. M. Vogels, J. R. Abo-Shaeer, A. P. Chikkatur, and W. Ketterle, *Phys. Rev. Lett.* **85**, 2228 (2000).
- [41] C. Raman, R. Onofrio, J. M. Vogels, J. R. Abo-Shaeer, and W. Ketterle, *J. Low Temp. Phys.* **122**, 99 (2001).
- [42] S. Inouye, S. Gupta, T. Rosenband, A. P. Chikkatur, A. Görlitz, T. L. Gustavson, A. E. Leanhardt, D. E. Pritchard, and W. Ketterle, *Phys. Rev. Lett.* **87**, 080402 (2001).
- [43] P. Engels and C. Atherton, *Phys. Rev. Lett.* **99**, 160405 (2007).
- [44] T. W. Neely, E. C. Samson, A. S. Bradley, M. J. Davis, and B. P. Anderson, *Phys. Rev. Lett.* **104**, 160401 (2010).
- [45] S. Burger, K. Bongs, S. Dettmer, W. Ertmer, K. Sengstock, A. Sanpera, G. V. Shlyapnikov, and M. Lewenstein, *Phys. Rev. Lett.* **83**, 5198 (1999).
- [46] J. Denschlag, J. E. Simsarian, D. L. Feder, C. W. Clark, L. A. Collins, J. Cubizolles, L. Deng, E. W. Hagley, K. Helmerson, W. P. Reinhardt, S. L. Rolston, B. I. Schneider, and W. D. Phillips, *Science* **287**, 97 (2000).

- [47] K. W. Madison, F. Chevy, W. Wohlleben, and J. Dalibard, *Phys. Rev. Lett.* **84**, 806 (2000).
- [48] P. C. Haljan, I. Coddington, P. Engels, and E. A. Cornell, *Phys. Rev. Lett.* **87**, 210403 (2001).
- [49] J. R. Abo-Shaeer, C. Raman, J. M. Vogels, and W. Ketterle, *Science* **292**, 476 (2001).
- [50] B. E. Sherlock, M. Gildemeister, E. Owen, E. Nugent, and C. J. Foot, *Phys. Rev. A* **83**, 043408 (2011).
- [51] G. E. Marti, R. Olf, and D. M. Stamper-Kurn, *Phys. Rev. A* **91**, 013602 (2015).
- [52] L. Amico, M. Boshier, G. Birkl, A. Minguzzi, C. Miniatura, L. C. Kwek, D. Aghamalyan, V. Ahufinger, N. Andrei, A. S. Arnold, M. Baker, T. A. Bell, T. Bland, J. P. Brantut, D. Cassettari, F. Chevy, R. Citro, S. D. Palo, R. Dumke, M. Edwards, R. Folman, J. Fortagh, S. A. Gardiner, B. M. Garraway, G. Gauthier, A. Günther, T. Haug, C. Hufnagel, M. Keil, W. von Klitzing, P. Ireland, M. Lebrat, W. Li, L. Longchambon, J. Mompert, O. Morsch, P. Naldesi, T. W. Neely, M. Olshanii, E. Orignac, S. Pandey, A. Pérez-Obiol, H. Perrin, L. Piroli, J. Polo, A. L. Pritchard, N. P. Proukakis, C. Rylands, H. Rubinsztein-Dunlop, F. Scazza, S. Stringari, F. Tosto, A. Trombettoni, N. Victorin, D. Wilkowski, K. Xhani, and A. Yakimenko, Roadmap on atomtronics, [arXiv:2008.04439](https://arxiv.org/abs/2008.04439).
- [53] X. Antoine and R. Duboscq, *Comput. Phys. Commun.* **185**, 2969 (2014).
- [54] X. Antoine and R. Duboscq, *Comput. Phys. Commun.* **193**, 95 (2015).
- [55] If the circulation, $\oint v d\ell$, over a closed path around a point traversed in the anticlockwise direction is a positive multiple of 2π , we call that defect a vortex, while a negative multiple one is an antivortex.
- [56] X. Yu and A. S. Bradley, *Phys. Rev. Lett.* **119**, 185301 (2017).
- [57] Assuming the ground state density, $|\psi_{\text{gs}}(r, \vartheta)|^2$, in the definition of $P(r)$ can be well approximated by a nonzero constant, ρ_0 , for $R_1 \leq r \leq R_2$ and zero otherwise. By geometrical argument and due to the normalization of $P(r)$, one may easily obtain $\rho_0^{-1} = \pi(R_2^2 - R_1^2)$, hence $P^3(r) = 2r/(R_2^2 - R_1^2)$. Then the two different averages are expressed as
- $$\frac{1}{\bar{r}^2} = \frac{1}{R_1^2} \times \left(\frac{3}{2}\right)^2 \left(\frac{1 + \chi}{1 + \chi + \chi^2}\right)^2$$
- $$\frac{1}{\bar{r}^2} = \frac{1}{R_1^2} \times \frac{2\ln(\chi)}{\chi^2 - 1},$$
- using the dimensionless ratio of the two radii, $\chi = R_2/R_1 \geq 1$. The difference between these averages reaches its maximum around $\chi \approx 3$, where it approximately becomes $\sim 0.06/R_1^2$. We neglected this difference in our simulation.
- [58] G. Watanabe, F. Dalfovo, F. Piazza, L. P. Pitaevskii, and S. Stringari, *Phys. Rev. A* **80**, 053602 (2009).
- [59] V. Hakim, *Phys. Rev. E* **55**, 2835 (1997).
- [60] A. M. Leszczyszyn, G. A. El, Y. G. Gladush, and A. M. Kamchatnov, *Phys. Rev. A* **79**, 063608 (2009).
- [61] N. Bogolubov, *J. Phys. (USSR)* **11**, 23 (1947).
- [62] P.-G. d. Gennes, *Superconductivity of Metals and Alloys* (Advanced Book Program, Perseus Books, Reading, MS, 1999).
- [63] D. A. W. Hutchinson, E. Zaremba, and A. Griffin, *Phys. Rev. Lett.* **78**, 1842 (1997).
- [64] D. A. W. Hutchinson and E. Zaremba, *Phys. Rev. A* **57**, 1280 (1998).
- [65] R. Dubessy, T. Liennard, P. Pedri, and H. Perrin, *Phys. Rev. A* **86**, 011602(R) (2012).